# Pion-induced spallation of copper across the (3,3) resonance

C. J. Orth, B. J. Dropesky, R. A. Williams, and G. C. Giesler
*Los Alamos Scientific Laboratory, Los Alamos, New Mexico 87545*

J. Hudis
*Chemistry Department, Brookhaven National Laboratory, Upton, New York 11973*

(Received 13 April 1978)

Cross sections for about two dozen radioactive spallation products have been measured for 50-, 100-, 190-, and 350-MeV $\pi^{\pm}$ and for 200- and 350-MeV proton interactions with copper. Sums of measured pion-induced cross sections at 50 and 350 MeV are about the same as for protons of 200 and 590 MeV, respectively. However, at 100 and 190 MeV, nearer to the (3,3) pion-nucleon resonance, these pion-induced cross section sums are 50 to 75% greater than those for protons of similar total energy. Ratios of the $\pi^-$ to $\pi^+$ cross sections are greater than unity for neutron-rich products and less than unity for neutron-deficient products at all four energies, indicating that pion absorption is a substantial reaction mode, even at 190 and 350 MeV. At 100 MeV, and especially at 50 MeV, absorption appears to dominate over inelastic scattering and the $\sigma_{\pi^-}/\sigma_{\pi^+}$ ratios are noticeably changed from those at the higher energies. The intranuclear cascade plus evaporation codes reproduce the proton cross sections fairly well. The pion version of the intranuclear cascade code reproduces the pion results quite well at 350 MeV, but it underestimates them significantly at 50 and 100 MeV.

[NUCLEAR REACTIONS Cu ($\pi^{\pm}$, spallation) and Cu ($p$, spallation), $E_{\pi^{\pm}} = 50$, 100, 190, 350 MeV, $E_p = 200$, 350 MeV. Production cross sections for radioactive residual nuclei. Comparison with intranuclear cascade plus evaporation calculations.]

## I. INTRODUCTION

Spallation reactions of medium energy protons with complex nuclei have been studied extensively,[1-7] especially in recent years with the availability of high resolution $\gamma$-ray spectrometers. The reaction is presumed to begin with an interaction of the incoming proton with a target nucleon; successive scattering of the original and struck nucleon then initiates an intranuclear cascade. The residual nucleus is thus left in an excited state and proceeds to dissipate this excitation energy, on a much slower time scale, by the emission of nucleons, small fragments, and $\gamma$ rays. The most successful model calculations treat this complicated cascade by following the multiple scattering of the nucleons using a Monte Carlo technique, and the residual excited nucleus is treated with an evaporation code. These calculations, such as VEGAS[8-10] and DFF,[11] reached a degree of sophistication such that over an energy range of about 100–1000 MeV they can reproduce proton results rather well.

Intranuclear production, scattering, and reabsorption of pions plays an important role in the successful predictive capabilities of these calculations especially at incident proton energies $\geq 1$ GeV. The most notable effect is the increased conversion of incident proton kinetic energy to nuclear excitation energy, because the reabsorption of pions transfers not only their kinetic energy but also their rest mass energy (140 MeV) to the nucleus. The availability of charged pions as incident projectiles now permits testing and refinement of the nuclear models and pion reaction mechanisms used in the calculations.

In the past, activation studies of pion-induced reactions have been severely hindered by the lack of sufficient beam intensity. Some early activation work with thick targets of Br, Zn, As, I, and Hg, in which relatively low energy $\pi^-$ were essentially stopped in the targets, has been published.[12-16] Some exploratory work with 215- to 373-MeV $\pi^-$ on Cu has been reported by Reeder[3] and comparison studies of 65-MeV $\pi^+$ and $\pi^-$ and 205-MeV proton reactions with Cu have been published.[1] In this last work a dozen products were measured and evidence for strong pion absorption at 65 MeV was observed. These pions with total energy, rest mass plus kinetic energy, of about 205 MeV, put more excitation energy into the Cu nucleus than do 205-MeV protons.

With the advent of the new high-intensity, medium-energy accelerators this lack of pion beam intensity has been remedied and the large pion fluxes at the Clinton P. Anderson Los Alamos Meson Physics Facility (LAMPF) have been used to study the interaction of fast $\pi^+$ and $\pi^-$ beams

 

with copper targets. Copper was selected for three reasons: (i) considerable medium-energy proton data with which to compare the pion results are in the literature; (ii) about two-dozen $\gamma$-emitting radioactive products can be measured by direct high-resolution $\gamma$ spectrometry on the irradiated foils; and (iii) copper is a target material readily available in high purity.

The primary incentive for this study was to test the validity of the model for pion-induced reactions used in the ISOBAR version[17] of the VEGAS intranuclear cascade code. In this work, we have measured cross sections for $\gamma$-emitting products from the interactions of 50-, 100-, 190-, and 350-MeV $\pi^+$ and $\pi^-$ with natural Cu. We have also made similar measurements with 200- and 350-MeV protons and made use of 590-MeV proton data in the literature[7] for comparison purposes. Cross sections for about two-dozen products are reported and compcompared with calculated results from the ISOBAR version of VEGAS.

## II. EXPERIMENTAL

The pion irradiations at 100 MeV and above were carried out at the $P^3$ (pions for particle physics) channel and the 50-MeV runs were conducted at the LEP (low energy pion) channel at LAMPF. These irradiations were performed over a period of time during which the primary proton beam was increased from 7 to 225 $\mu$A. The targets were exposed to pions for periods ranging from one to four hours. The pion irradiation conditions are given in Table I.

The targets were electrolytically refined, 3.8-cm diam copper disks (Cu purity >99.8%). The thicknesses ranged from 1.8 g cm$^{-2}$ in the earlier runs to 0.4 g cm$^{-2}$ in the later runs at higher beam intensities.

The pion fluence was determined by activation of Pilot B (20.4-min $^{11}$C) and Al and Si (110-min $^{18}$F and 15-h $^{24}$Na) monitor disks. The excitation functions for the first reaction have been reported[18] and recently the excitation functions for the production of $^{18}$F and $^{24}$Na from Al and Si have been measured at LAMPF.[19] In the $P^3$ channel a momentum bite ($\Delta p/p$) of 6% was selected in order to provide high pion intensity. At the LEP channel $\Delta p/p$ was set to 2%. At 50 MeV in the LEP channel and at 100 MeV in the $P^3$ channel the pion beams, especially $\pi^-$, contained a considerable electron contamination; however, electron-induced activation yielding the products measured is negligible.[20] At 350 MeV, the $\pi^+$ beam contained ~1% proton contamination despite the fact that proton degraders and absorbers were placed in the channel. This proton contribution was also insignificant. Secondary neutrons coming down the channel were not detectable. At a given energy, the $\pi^+$ flux was generally 3 to 4 times larger than the $\pi^-$ flux due to the larger $\pi^+$ production by protons on the graphite production targets.

Secondary neutrons and protons generated in the relatively thick Cu targets by the pion interactions undoubtedly cause some enhancement of products close in $Z$ to that of the target, especially in $Z+1$ products from $\pi^+$ irradiations. In another study, to be reported later,[21] the observed amount of $^{61}$Cu from stopped $\pi^-$ interactions with Cu suggests that as much as 5% of the reported $^{61}$Cu cross sections for fast pions may have come from secondary reactions.

Within 15 minutes after an irradiation, the target and monitor disks were removed to a low background, shielded environment for counting the induced radioactivity. In the course of this work, three different Ge(Li) $\gamma$-ray spectrometer systems were used to collect the $\gamma$-ray spectra from

TABLE I. Pion irradiation conditions.

| Run | Energy (MeV) and charge | Channel | Proton current ($\mu$A) | Pion flux (sec$^{-1}$) | Beam monitor and cross section (mb) |
|---|---|---|---|---|---|
| 1 | 190, $\pi^+$ | $P^3$ | 7 | $10^7$ | C($^{11}$C) 43 |
| 2 | 190, $\pi^+$ | $P^3$ | 10 | $1.4\times10^7$ | Al($^{18}$F) 12.8 |
| 3 | 190, $\pi^-$ | $P^3$ | 10 | $3\times10^6$ | Al($^{18}$F) 11.2 |
| 4 | 350, $\pi^+$ | $P^3$ | 97 | $5\times10^8$ | Si($^{24}$Na) 4.9 |
| 5 | 350, $\pi^-$ | $P^3$ | 97 | $3.2\times10^7$ | Al($^{24}$Na) 12.6 |
| 6 | 190, $\pi^-$ | $P^3$ | 97 | $3\times10^7$ | Al($^{24}$Na) 23.4 |
| 7 | 100, $\pi^+$ | $P^3$ | 97 | $4.5\times10^7$ | Al($^{24}$Na) 12.6 |
| 8 | 100, $\pi^-$ | $P^3$ | 97 | $1.2\times10^7$ | Al($^{24}$Na) 23.4 |
| 9 | 50, $\pi^+$ | LEP | 225 | $1.2\times10^7$ | Al($^{18}$F) 4.6 |
| 10 | 50, $\pi^-$ | LEP | 225 | $5\times10^6$ | Al($^{18}$F) 4.6<br>Al($^{24}$Na) 13.0 |

the Cu targets. The photopeak efficiencies of these detectors were calibrated using National Bureau of Standards $^{241}$Am, $^{228}$Th, and mixed $\gamma$-ray standard sources. The energy resolution full width at half maximum (FWHM) of these detectors was ~2.2 keV for the $^{60}$Co 1332-keV photopeak.

Corrections were made for photon absorption in the relatively thick copper disks and also for the large source diameter (3.8 cm) vs the point sources of the calibration standards.

The pion fluence in the first run was measured by placing a 0.32-cm thick × 3.8-cm diam Pilot B scintillator disk in front contact with the Cu target. The induced $^{11}$C disintegration rate was determined by $\beta^+$-$\gamma$ (511 keV) coincidence counting by coupling the plastic disk to a photomultiplier tube which was then mounted so that the disk was in contact with a 7.6-cm × 7.6-cm NaI(Tl) scintillator unit which detected the annihilation photons. The system is described in Ref. 18.

The $^{18}$F disintegration rate in Al or Si monitor disks was determined by $\gamma$-$\gamma$ coincidence counting of the annihilation radiation with a pair of 7.6-cm × 7.6-cm NaI(Tl) scintillators which was calibrated by the use of activated Pilot B disks whose $^{11}$C absolute disintegration rate was determined by the $\beta^+$-$\gamma$ coincidence counting system described above.

The $^{24}$Na disintegration rates in Al and Si monitor disks in the later high pion fluence runs were determined by measuring the photon spectrum intensity between 1.3 and 2.9 MeV with a 7.6-cm × 7.6-cm NaI(Tl) spectrometer. The counting efficiency was determined from specially prepared $^{24}$Na standards whose geometry was identical to the monitors. The standards were prepared from $^{24}$Na solutions which were standardized with calibrated Ge(Li) detectors.

For the purpose of comparison, we have also measured cross sections of similar products from the interaction of 200- and 350-MeV protons on copper. In this work we also compare our pion data with 590-MeV proton cross sections measured previously in a study involving two of the present authors.[7] The 200-MeV proton irradiations and subsequent $\gamma$-ray measurements were carried out at BNL while the 350-MeV proton work was done at LAMPF. Duplicate irradiations were performed at 350 MeV and one set of a pair of irradiated foils was also counted at BNL for interlaboratory comparison of $\gamma$-spectrometry techniques. The techniques were essentially identical to the pion measurements except thinner and smaller foils were used. The proton fluences were determined from the amount of $^{24}$Na induced in Al monitor foils. The $^{24}$Na monitor cross sections used were taken from the tables given by Cumming.[22]

TABLE II. Nuclear data used to calculate cross sections.

| Nuclide | Half-life | $\gamma$-ray energy (keV) | $\gamma$-rays/disintegration |
|---|---|---|---|
| $^{62}$Zn | 9.15 h | 597 | 0.26 |
| $^{61}$Cu | 3.37 h | 283 | 0.13 |
| $^{57}$Ni | 36 h | 1378 | 0.349 |
| $^{55}$Co | 17.9 h | 931 | 0.73 |
| $^{56}$Co | 78.5 day | 847 | 1.00 |
| $^{57}$Co | 271.4 day | 122 | 0.86 |
| $^{58}$Co | 71.3 day | 811 | 1.00 |
| $^{61}$Co | 1.65 h | 67 | 0.90 |
| $^{52}$Fe | 8.3 h | 168 | 1.00 |
| $^{59}$Fe | 44.6 day | 1099/1292 | 0.565/0.432 |
| $^{52}$Mn | 5.63 day | 1434 | 1.00 |
| $^{54}$Mn | 312.4 day | 835 | 1.00 |
| $^{56}$Mn | 2.58 h | 847 | 1.00 |
| $^{48}$Cr | 21.6 h | 308 | 0.99 |
| $^{49}$Cr | 42 m | 91 | 0.539 |
| $^{51}$Cr | 27.7 day | 320 | 0.098 |
| $^{48}$V | 16.0 day | 983 | 1.00 |
| $^{44}$Sc$^m$ | 58.6 h | 1157/270 | 1.072/0.86 |
| $^{44}$Sc$^g$ | 3.93 h | 1157 | 1.00 |
| $^{46}$Sc | 83.9 day | 889 | 1.00 |
| $^{47}$Sc | 3.41 day | 159 | 0.73 |
| $^{48}$Sc | 43.7 h | 1037 | 1.00 |
| $^{42}$K | 12.4 h | 1525 | 0.18 |
| $^{43}$K | 22.2 h | 373/617 | 0.85/0.66 |
| $^{41}$Ar | 1.83 h | 1294 | 1.00 |

TABLE III. Cross sections for $\pi^+$- induced spallation of copper at 50, 100, 190, and 350 MeV.

| Nuclide | | Type | Measured (mb) 50 | 100 | 190 | 350 | Calculated (mb) 50 | 100 | 190 | 350 |
|---|---|---|---|---|---|---|---|---|---|---|
| 9.15 h | $^{62}$Zn | I | 1.8 ±0.3 | 1.9 ±0.4 | 1.9 ±0.4 | 0.54±0.10 | 2.7 ±0.8 | | | |
| 3.37 h | $^{61}$Cu | C | 10.3 ±0.9 | 32 ±3 | 24 ±3 | 14 ±1 | 19.6 ±2.2 | 48 ±4 | 27 ±3 | 20.4 ±2.4 |
| 36 h | $^{57}$Ni | C | 2.35±0.41 | 2.5 ±0.4 | 2.2 ±0.4 | 1.2 ±0.1 | 3.6 ±1.0 | 4.4 ±1.1 | 7.0 ±1.4 | 3.3 ±0.9 |
| 17.9 h | $^{55}$Co | C | 2.97±0.40 | 3.9 ±0.4 | 2.9 ±0.5 | 2.0 ±0.2 | 5.2 ±1.1 | 5.7 ±1.2 | 8.8 ±1.6 | 3.8 ±1.0 |
| 78.5 day | $^{56}$Co | C | 13.3 ±3.0 | 23 ±4 | 21 ±4 | 12 ±2 | 14 ±2 | 22 ±3 | 30 ±3 | 15 ±2 |
| 271.4 day | $^{57}$Co | C | 44 ±4 | 53 ±5 | 55 ±6 | 30 ±4 | 19 ±3 | 36 ±3 | 49 ±3.4 | 25 ±2.5 |
| 71.3 day | $^{58}$Co | I | 35 ±4 | 54 ±4 | 62 ±6 | 33 ±3 | 12.6 ±1.8 | 32.3 ±3.0 | 41.1 ±3.4 | 21.0 ±2.4 |
| 1.65 h | $^{61}$Co | C(I) [a] | 1.49±0.45 | 3.7 ±0.7 | 5.7 ±0.7 | 4.4 ±0.9 | 0.58±0.38 | 0.94±0.50 | 1.0 ±0.5 | 2.5 ±0.8 |
| 8.3 h | $^{52}$Fe | C | 0.23±0.04 | 0.39±0.05 | 0.36±0.09 | 0.24±0.03 | 0.63±0.40 | 0.94±0.50 | 1.0 ±0.5 | 0.90±0.51 |
| 44.6 day | $^{59}$Fe | C(I) | | 1.5 ±0.7 | 2.3 ±1.0 | 2.3 ±1.0 | 0.23±0.23 | 0.84±0.48 | 2.9 ±0.9 | 1.2 ±0.6 |
| 5.63 day | $^{52}$Mn | C | 6.1 ±0.8 | 13 ±2 | 12.5 ±2 | 9.8 ±1.0 | 12.5 ±1.7 | 21 ±3 | 23 ±3 | 16.0 ±2.1 |
| 312.4 day | $^{54}$Mn | I | 23.5 ±3.5 | 35 ±4 | 40 ±5 | 26 ±3 | 10.7 ±1.6 | 17.3 ±2.1 | 25.8 ±2.7 | 16.4 ±2.2 |
| 2.58 h | $^{56}$Mn | C | 2.26±0.24 | 3.4 ±0.4 | 4.8 ±0.8 | 3.3 ±0.3 | 1.16±0.54 | 1.9 ±0.7 | 4.9 ±1.2 | 2.9 ±0.9 |
| 21.6 h | $^{48}$Cr | C | 0.17±0.07 | 0.32±0.07 | 0.43±0.10 | 0.47±0.10 | 0.23±0.24 | 0.38±0.32 | 0.95±0.51 | 1.4 ±0.5 |
| 42 m | $^{49}$Cr | C | 1.46±0.34 | 2.9 ±0.4 | 3.4 ±1.6 | 3.8 ±1.0 | 2.5 ±0.8 | 4.6 ±1.1 | 7.8 ±1.4 | 7.4 ±1.4 |
| 27.7 day | $^{51}$Cr | C | 18.1 ±5.4 | 33 ±4 | 40 ±5 | 28 ±3 | 12.8 ±1.8 | 23 ±3 | 33 ±3 | 27 ±3 |
| 16.0 day | $^{48}$V | C | 2.93±0.37 | 8.9 ±1.2 | 11.7 ±1.6 | 12 ±1 | 5.0 ±1.1 | 9.0 ±1.5 | 15 ±2 | 17 ±2 |
| 3.93 h | $^{44}$Sc$^{g}$ | I | 0.39±0.08 | 2.4 ±0.5 | 5.1 ±1.2 | 6.6 ±1.0 | 0.25±0.25 | 1.4 ±0.6 | 5.3 ±1.2 | 12.1 ±1.8 |
| 58.6 h | $^{44}$Sc$^{m}$ | I | | | | | | | | |
| 83.8 day | $^{46}$Sc | I | | 2.1 ±0.6 | 2.1 ±1.2 | 5.3 ±0.6 | 0.43±0.33 | 1.1 ±0.5 | 4.4 ±1.1 | 6.6 ±1.4 |
| 3.41 day | $^{47}$Sc | C | 0.39±0.09 | 0.93±0.22 | 1.4 ±0.8 | 1.8 ±0.5 | 0.35±0.30 | 1.1 ±0.5 | 2.8 ±0.8 | 3.6 ±1.0 |
| 43.7 h | $^{48}$Sc | I | | 0.17±0.06 | 0.50±0.06 | 0.52±0.15 | | 0.22±0.24 | 1.2 ±0.6 | 2.0 ±0.8 |
| 12.4 h | $^{42}$K | I | | | | 1.5 ±0.4 | | 0.14±0.19 | 0.84±0.48 | 2.4 ±0.8 |
| 22.2 h | $^{43}$K | C | | | 0.36±0.15 | 0.52±0.10 | | | 0.36±0.32 | 1.4 ±0.6 |
| 1.83 h | $^{41}$Ar | C | | 0.08±0.03 | | 0.21±0.05 | | | 0.14±0.13 | 0.7 ±0.8 |
| | | $\sum$ (mb) | 167 | 276 | 300 | 200 | 123 | 234 | 305 | 214 |

[a] C(I) = The yields reported are predominantly independent, but with a minor contribution from other members of the chain.

TABLE IV. Cross sections for $\pi^-$-induced spallation of copper at 50, 100, 190, and 350 MeV.

| Nuclide | | Yield type | Measured (mb) 50 | 100 | 190 | 350 | Calculated (mb) 50 | 100 | 190 | 350 |
|---|---|---|---|---|---|---|---|---|---|---|
| 3.37 h | $^{61}$Cu | I | 8.0 ±1.0 | 27.7 ±3.0 | 29 ±3 | 15 ±2 | 17.1 ±2.3 | 39.2 ±3.5 | 28.3 ±2.9 | 13.5 ±2.0 |
| 36 h | $^{57}$Ni | C | 0.61 ±0.17 | 0.80 ±0.20 | 1.4 ±0.2 | 1.1 ±0.2 | 0.97 ±0.56 | 1.4 ±0.6 | 4.2 ±1.1 | 1.8 ±0.7 |
| 17.9 h | $^{55}$Co | C | 1.03 ±0.10 | 1.67 ±0.18 | 2.0 ±0.3 | 1.3 ±0.2 | 1.00 ±0.57 | 1.9 ±0.8 | 5.0 ±1.2 | 2.5 ±0.8 |
| 78.5 day | $^{56}$Co | C | 8.7 ±2.1 | 15.0 ±2.6 | 18 ±3 | 10.4 ±2.0 | 8.0 ±1.6 | 13 ±2 | 24 ±3 | 11.4 ±1.8 |
| 271.4 day | $^{57}$Co | C | 35 ±5 | 47 ±6 | 53 ±5 | 28 ±4 | 16.8 ±2.3 | 29 ±3 | 48 ±4 | 1.8 ±2 |
| 71.3 day | $^{58}$Co | I | 48 ±5 | 67 ±7 | 68 ±7 | 32 ±3 | 22.7 ±2.7 | 37.9 ±3.4 | 45.4 ±3.7 | 19.7 ±2.4 |
| 1.65 h | $^{61}$Co | C | 10.7 ±1.2 | 13 ±3 | 11.3 ±1.6 | 6.1 ±0.8 | 5.3 ±1.2 | 8.2 ±1.6 | 7.9 ±1.5 | 2.6 ±0.9 |
| 8.3 h | $^{52}$Fe | C | 0.068 ±0.024 | 0.15 ±0.04 | 0.16 ±0.10 | 0.15 ±0.05 | 0.032 ±0.102 | 0.15 ±0.21 | 0.12 ±0.19 | 0.18 ±0.22 |
| 44.6 day | $^{59}$Fe | C | 6.2 ±1.2 | 7.3 ±1.0 | 6.3 ±2.0 | 3.4 ±0.8 | 4.0 ±1.1 | 5.7 ±1.3 | 5.6 ±1.3 | 2.6 ±0.9 |
| 5.63 day | $^{52}$Mn | C | 5.0 ±0.8 | 9.1 ±1.6 | 11 ±2 | 8.4 ±0.9 | 5.1 ±1.3 | 8.5 ±1.6 | 14.5 ±2.1 | 11.2 ±1.8 |
| 312.5 day | $^{54}$Mn | I | 38 ±6 | 53 ±6 | 53 ±4 | 35 ±4 | 20.0 ±2.5 | 22.5 ±2.6 | 33.2 ±3.1 | 18.3 ±2.3 |
| 2.58 h | $^{56}$Mn | C | 9.0 ±2.0 | 11.6 ±1.6 | 9.4 ±0.8 | 7.4 ±0.8 | 7.8 ±1.6 | 7.8 ±1.5 | 10.8 ±1.8 | 3.8 ±1.0 |
| 21.6 h | $^{48}$Cr | C | | <0.20 | 0.25 ±0.06 | 0.26 ±0.05 | | 0.031 ±0.097 | 0.09 ±0.16 | 0.44 ±0.36 |
| 42 m | $^{49}$Cr | C | 0.61 ±0.20 | 1.8 ±0.3 | 2.4 ±0.5 | 2.6 ±0.5 | 0.39 ±0.35 | 0.82 ±0.50 | 2.8 ±0.9 | 3.8 ±1.0 |
| 27.7 day | $^{51}$Cr | C | 15 ±3 | 34 ±4 | 39 ±4 | 25 ±3 | 9.8 ±1.9 | 17.5 ±2.3 | 25 ±3 | 22 ±3 |
| 16.0 day | $^{48}$V | C | 2.06 ±0.50 | 5.3 ±1.2 | 10 ±1 | 10 ±1 | 1.4 ±0.7 | 3.6 ±1.0 | 8.2 ±1.6 | 11.0 ±1.8 |
| 3.93 h | $^{44}$Sc$^{g}$ | I | | 1.78 ±0.25 | 4.4 ±1.0 | 6.4 ±1.2 | 0.1 ±0.18 | 0.73 ±0.47 | 3.3 ±1.0 | 6.4 ±1.5 |
| 58.6 h | $^{44}$Sc$^{m}$ | I | | | | | | | | |
| 83.8 day | $^{46}$Sc | I | | 4.4 ±0.8 | 6.4 ±2.2 | 7.3 ±0.9 | 0.94 ±0.55 | 2.7 ±0.9 | 6.0 ±1.3 | 10.1 ±1.7 |
| 3.41 day | $^{47}$Sc | C | 1.0 ±0.2 | 2.0 ±0.5 | 3.2 ±0.5 | 3.3 ±0.8 | 1.6 ±0.6 | 3.5 ±0.9 | 7.0 ±1.3 | 6.7 ±1.4 |
| 43.7 h | $^{48}$Sc | I | 0.39 ±0.16 | 0.81 ±0.09 | 0.98 ±0.21 | 1 ±0.3 | 1.7 ±0.7 | 3.1 ±1.0 | 3.7 ±1.1 | 4.1 ±1.1 |
| 12.4 h | $^{42}$K | I | | | 2.1 ±0.5 | 2.2 ±0.3 | | 0.46 ±0.37 | 1.1 ±0.6 | 4.2 ±1.1 |
| 22.2 h | $^{43}$K | C | | 0.29 ±0.08 | 0.7 ±0.1 | 0.9 ±0.2 | 0.07 ±0.07 | 0.15 ±0.21 | 1.0 ±0.6 | 2.5 ±0.9 |
| 1.83 h | $^{41}$Ar | C | | | 0.23 ±0.09 | 0.5 ±0.1 | | | 0.6 ±0.4 | 3.3 ±1.0 |
| | | $\sum$ (mb) | 190 | 298 | 332 | 208 | 122 | 208 | 286 | 183 |

TABLE V. Cross sections for proton-induced spallation of copper at 200, 350, and 590 MeV.

| Nuclide | | Yield type | Measured (mb) 200 | 350 | 590 [a] | Calculated (mb) 200 | 350 | 590 |
|---|---|---|---|---|---|---|---|---|
| 9.15 h | $^{62}$Zn | I | 2.4 ±1.1 | 1.1 ±0.3 | 0.60±0.15 | 3.0 ±0.9 | 2.7 ±0.8 | 1.9 ±0.7 |
| 3.37 h | $^{61}$Cu | C | 25 ±3 | 20 ±3 | 17.5 ±2.0 | 34.0 ±3.1 | 28 ±3 | 19.7 ±2.2 |
| 36 h | $^{57}$Ni | C | 1.7 ±0.2 | 1.36±0.21 | 1.07±0.11 | 5.44±1.23 | 4.6 ±1.1 | 2.0 ±0.8 |
| 17.9 h | $^{55}$Co | C | 2.0 ±0.2 | 2.1 ±0.3 | 1.70±0.10 | 6.4 ±1.4 | 5.36±1.26 | 2.19±0.77 |
| 78.5 day | $^{56}$Co | C | 12.4 ±1.3 | 11.6 ±1.4 | 10.2 ±0.7 | 21.7 ±2.5 | 17.6 ±1.7 | 14.0 ±2.1 |
| 271.4 day | $^{57}$Co | C | 37.5 ±4.0 | 34.9 ±3.6 | 29.9 ±2.0 | 37.3 ±3.1 | 29.2 ±2.7 | 24.6 ±2.6 |
| 71.3 day | $^{58}$Co | I | 44.6 ±5.0 | 38.4 ±4.2 | 30.0 ±2.6 | 28.5 ±2.8 | 22.8 ±2.5 | 15.5 ±2.1 |
| 1.65 h | $^{61}$Co | C | | 3.4 ±0.7 | | 2.8 ±0.9 | 2.4 ±0.8 | 5.0 ±1.2 |
| 8.3 h | $^{52}$Fe | C | 0.10±0.02 | 0.22±0.05 | 0.27±0.03 | 0.50±0.37 | 0.59±0.41 | 0.79±0.48 |
| 4.6 day | $^{59}$Fe | C | 1.3 ±0.13 | 1.5 ±0.3 | 1.64±0.20 | 1.43±0.66 | 2.7 ±1.1 | 2.3 ±0.8 |
| 5.63 day | $^{52}$Mn | C | 5.56±0.60 | 8.3 ±1.1 | 9.3 ±0.6 | 12.3 ±2.0 | 14.6 ±2.0 | 19.2 ±2.3 |
| 312.5 day | $^{54}$Mn | I | 17.4 ±1.8 | 21.6 ±2.0 | 21.8 ±1.2 | 16.4 ±2.1 | 17.2 ±2.1 | 17.9 ±2.3 |
| 2.58h | $^{56}$Mn | C | 2.3 ±0.3 | 3.2 ±0.6 | 3.6 ±0.6 | 3.7 ±1.0 | 2.9 ±0.9 | 2.0 ±0.7 |
| 21.6 h | $^{48}$Cr | C | 0.07±0.01 | 0.23±0.06 | 0.30±0.02 | 0.03±0.09 | 0.51±0.35 | 1.0 ±0.5 |
| 42 m | $^{49}$Cr | C | 0.74±0.08 | 2.3 ±0.4 | | 1.65±0.75 | 3.6 ±0.9 | 8.9 ±1.6 |
| 27.7 day | $^{51}$Cr | C | 12.2 ±1.3 | 21 ±3 | 26.9 ±1.8 | 14.7 ±1.0 | 17.6 ±1.8 | 24.1 ±2.4 |
| 16.0 day | $^{48}$V | C | 2.4 ±0.3 | 6.6 ±1.0 | 9.53±0.65 | 2.8 ±0.9 | 18.8 ±1.2 | 14.9 ±2.1 |
| 3.93 h | $^{44}$Sc$^{g}$ | I | 0.33±0.04 | 2.73±0.35 | 6.6 ±1.1 | 0.25±0.26 | 2.6 ±0.9 | 10.8 ±1.8 |
| 58.6 h | $^{44}$Sc$^{m}$ | I | | | | | | |
| 83.8 day | $^{46}$Sc | I | 0.61±0.07 | 2.46±0.26 | 4.92±0.26 | 0.06±0.13 | 3.0 ±0.9 | 7.2 ±1.4 |
| 3.41 day | $^{47}$Sc | C | 0.36±0.04 | 1.2 ±0.2 | 1.90±0.13 | 0.03±0.09 | 1.9 ±0.8 | 3.6 ±1.1 |
| 43.7 h | $^{48}$Sc | I | 0.07±0.01 | 0.25±0.06 | 0.48±0.04 | | 1.27±0.60 | 1.8 ±0.7 |
| 12.4 h | $^{42}$K | C | 0.03±0.01 | 0.54±0.12 | 1.52±0.08 | | 0.80±0.47 | 3.3 ±1.0 |
| 22.2 h | $^{43}$K | C | | 0.20±0.05 | 0.55±0.07 | | 0.26±0.26 | 1.3 ±0.7 |
| 1.83 h | $^{41}$Ar | C | | 0.07±0.02 | | | 0.03±0.09 | 1.0 ±0.5 |
| | | $\sum$ (mb) [b] | 173 | 185(181) | 180(185) | 193(190) | 191(188) | 215(200) |

[a] 590-MeV data are taken from Ref. 7.

[b] $\sum$ (mb) in parentheses represent the sums of the same products as for 200-MeV protons.

## III. RESULTS

### A. Measurements

The half-life, $\gamma$-ray energy, and the number of photons per disintegration, which were used to compute the saturation disintegration rates of the measured species at the end of bombardment, are given in Table II. The cross sections for spallation products from $\pi^+$, $\pi^-$, and proton reactions with Cu are given in Tables III–V. The yields are listed as independent (I) or cumulative (C). The sums of the individual cross sections shown at the bottom of each column represent only about 25% of the total inelastic cross section, but they allow informative comparisons to be made among themselves and with the VEGAS calculations. Duplicate runs were performed at 190 MeV with both $\pi^+$ and $\pi^-$ as a check on reproducibility; this proved to be better than ±10% for all products and within ±5% for the products yielding high counting statistics.

The cross sections were computed from the ratio of the saturation disintegration rate of the spallation product to that of the monitor radionuclide whose cross section is known.

The uncertainties listed for the experimental data arise predominantly from determination of the photopeak intensities and from estimated uncertainties in the monitor cross sections. Smaller contributions arise from corrections for photon absorption in the target, extended source geometry of the target, photopeak efficiency of the detector, and variations in beam intensity during the irradiation.

### B. Calculations

The results of recent Monte Carlo intranuclear cascade calculations[23] with the ISOBAR version of VEGAS followed by DFF[11] evaporation calculations are included in Tables III–V. In the ISOBAR version a 1236Δ (pion-nucleon isobar) is formed when a pion and a nucleon scatter resonantly, as (1) $\pi + N \rightarrow \Delta$. The Δ then propagates through the nucleus as a single entity and can either decay back into a pion and nucleon, as (2) $\Delta \rightarrow \pi + N$ or strike another nucleon and go into two nucleons, as (3) $\Delta + N \rightarrow N_1 + N_2$. It is this scattering of the Δ, given by (3), that provides a mechanism for pion absorption. One of the primary aims of this work is to provide data to improve the ISOBAR model in order

to better predict the experimental observations. The original ISOBAR version has been modified to include an energy-dependent lifetime of the Δ, nonresonant scattering, and a form factor in the absorption calculations. Nonresonant scattering can occur in the isospin $\frac{1}{2}$ channel where no Δ is formed. The form factor reduces the absorption cross section because the pion-nucleon wave function becomes very small when two nucleons come too close to each other. Although these modifications have reduced the discrepancies between measured and calculated cross sections, there remains considerable discrepancy at lower pion energies where the calculation underestimates pion absorption. In general, 10000 cascades were followed and errors quoted for the calculated cross sections are statistical.

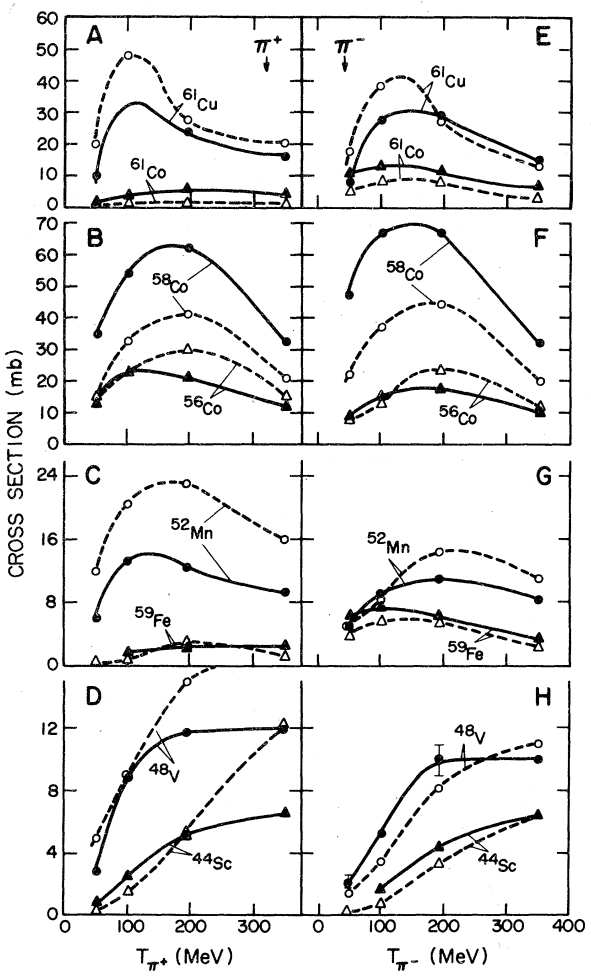


FIG. 1. Excitation functions for several representative spallation products from fast $\pi^+$ and $\pi^-$ reactions with Cu. The curves are drawn to aid the eye. Solid curves through measured points and dashed curves through ISOBAR-DFF calculated points.

## IV. DISCUSSION

### A. Comparison with previous pion measurements

Previous results for pion-induced spallation of copper are to be found in some exploratory work by Reeder with 215- to 373-MeV $\pi^-$ and a study by Garrett and Turkevich[1] in which they measured and compared cross sections from 65-MeV $\pi^+$ and $\pi^-$ and 205-MeV proton reactions. Reeder[3] reports data for $^{61}$Cu, $^{52,56}$Mn, and $^{52}$Fe, and only the $^{61}$Cu result agrees with ours within the quoted errors.

Interpolation of our cross section values to 65 MeV gives excellent agreement with the results of Garrett and Turkevich. One exception is $^{59}$Fe from $\pi^-$ interactions; they report a cross section that is an order of magnitude lower than we measure.

### B. General features and comparisons of the pion results

Most of the excitation functions for individual spallation products between $A = 51$ and 61, some of which are shown in Fig. 1, peak near incident $\pi^\pm$ energies of 170 MeV. The sums of the measured cross sections shown in Fig. 2 also peak

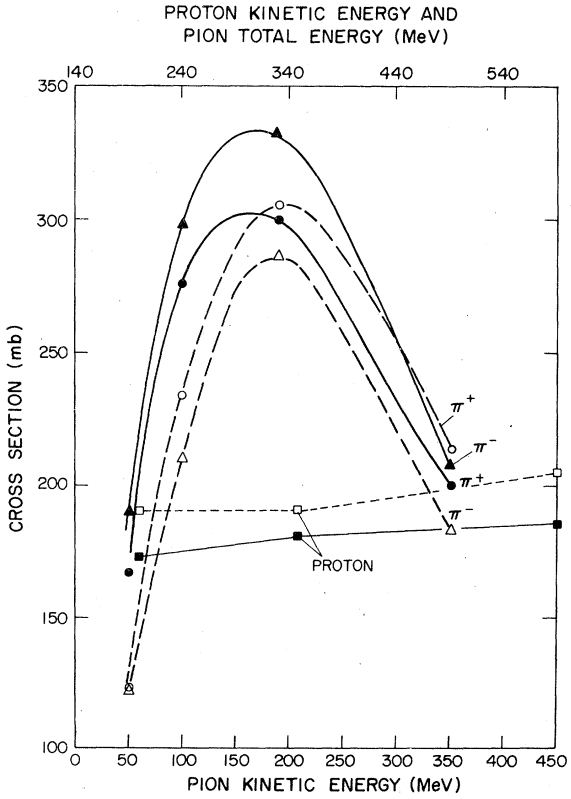


FIG. 2. Excitation functions for the sums of the cross sections given in Tables III–V. The curves are drawn to aid the eye. Solid curves through measured points and dashed curves through ISOBAR-DFF calculated points and ● and ○ for $\pi^+$; ▲ and △ for $\pi^-$; ■ and □ for protons.

near 170 MeV due to the fact that most of the cross section arises from products within ten mass units of the target. The influence of the (3,3) pion-nucleon resonance is thus apparent even in some reactions where the resonant process is only the first of many steps. However, the excitation functions of products that result from large excitation energy deposition such as $^{44}$Sc, $^{48}$V, and $^{49}$Cr increase rapidly to about 200 MeV and then either level off or increase more gradually to 350 MeV. At or near resonance the sums of the measured pion cross sections are about 50 to 75 % greater than those for protons of similar total energy ($T_{\pi^+}$ 140 MeV). Off resonance, at 50- and 350-MeV pion energies the sums of the cross sections we measure are quite similar to those for protons of kinetic energy similar to the pion total energy. At resonance the sums of the $\pi^-$ cross sections are about 10% larger than the sums of $\pi^+$.

The relative contributions of absorption and inelastic scattering as a function of pion kinetic energy can be obtained, on a qualitative basis, from the data of Tables III and IV. The effect can be most easily observed by plotting the $\sigma_{\pi^-}/\sigma_{\pi^+}$ ratios for neutron-rich and neutron-deficient products versus pion kinetic energy. While $\pi^-$ absorption increases the $N/Z$ ratio of the pion-plus-target system, the converse is true with $\pi^+$ absorption. The two cases shown in Fig. 3 demonstrate the point. The plots of $^{55}$Co (neutron deficient) and $^{61}$Co (neutron rich) and similar plots for other species that are not shown indicate that pion absorption is a strong mode of interaction at low energy. With increasing energy, as the resonance is approached, inelastic scattering becomes more important and appears to remain thus, although the cross sections themselves decrease above resonance.

In addition to the loss of pion kinetic energy in pion-nucleon scattering interactions, the absorption process can deposit up to an additional 140 MeV of excitation energy in the nucleus, and one major point of interest is the relative maximum amount of excitation energy imparted to the nucleus by pions and protons. This was obtained by plotting the independent isotopic yields of several product elements, where sufficient data exist (Sc, Cr, Mn, and Co), versus mass number. Plots of the interpolated cross-section maxima of the isotopic yields vs the mass number of the maxima, are shown in Fig. 4. These curves show a linear slope at large $\Delta A$, and the large $\Delta A$ products are the result of very high excitation energy deposited in the nucleus. A plot of the relative slopes of the linear portion of the mass yield curves between $A = 45$ and 49 for $\pi^-$ and protons against the particle kinetic energy is shown in Fig. 5.

The shift in the curves shows that the pion absorption process leads to higher excitation levels

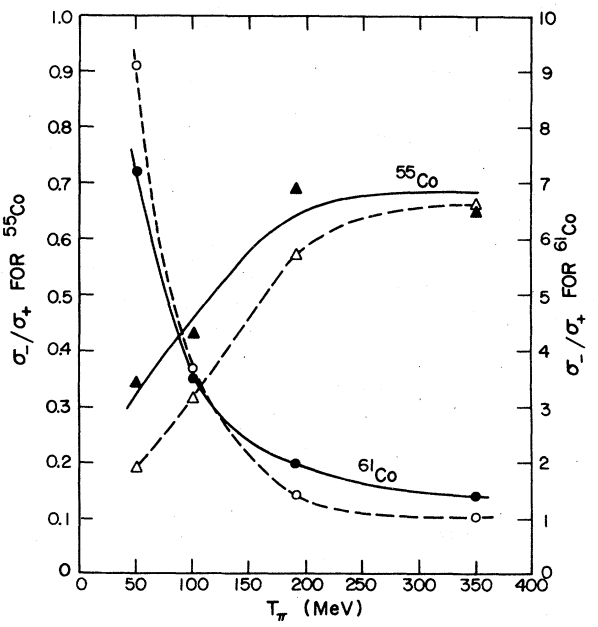


FIG. 3. Ratios of $\pi^-$ to $\pi^+$ cross sections for $^{55}$Co and $^{61}$Co from Cu as a function of pion kinetic energy. The curves are drawn to aid the eye. Solid curves through measured points and dashed curves through ISOBAR-DFF calculated points: ● and ○ for $^{61}$Co; ▲ and △ for $^{55}$Co.

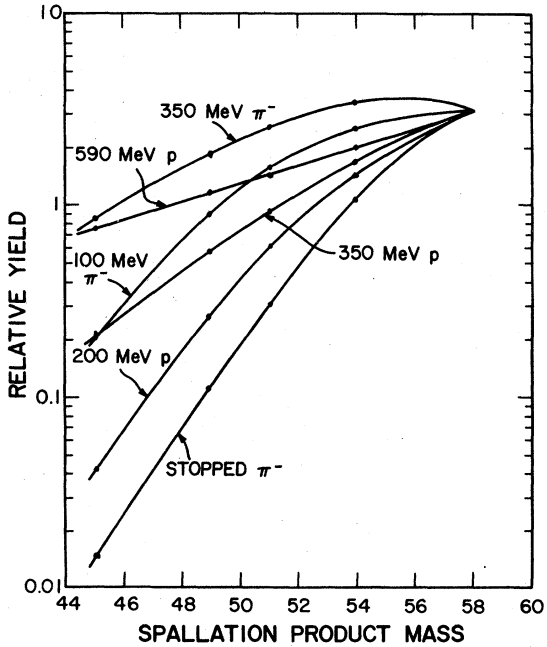


FIG. 4. Relative mass yield curves for $\pi^-$ and proton interactions with Cu. Smooth curves were drawn through the peaks of the isotopic yield curves determined experimentally for Sc, Cr, Mn, and Co, normalized at $^{58}$Co.

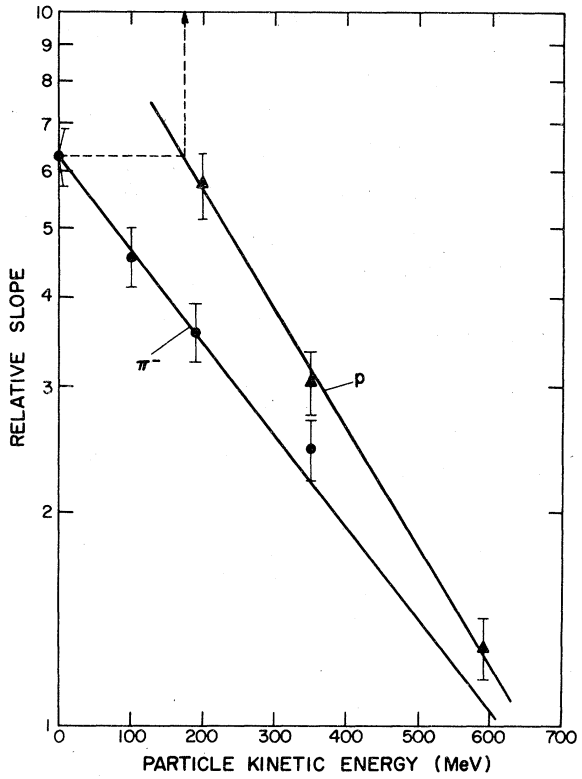


FIG. 5. Relative slopes of the linear portions (between $A=45$ and $A=49$) of the mass yield curves shown in Fig. 4. The dashed lines in the upper left corner are drawn to demonstrate that a stopped $\pi^-$ interaction imparts the same total excitation energy to a Cu nucleus as does a 170-MeV proton.

compared to protons of equal kinetic energy and that stopped pions are similar to protons with ~170 MeV of kinetic energy. We have chosen $\pi^-$ for this comparison because spallation yields have been measured for $\pi^-$ down to $T=0$ (stopped $\pi^-$ reactions) and they will be reported in a subsequent paper.[21]

Thus, at low kinetic energies, pions are efficiently absorbed and can transfer their rest mass energy into excitation. As the pion kinetic energy is increased, absorption decreases and inelastic scattering becomes the more important reaction channel.

### C. Comparison with VEGAS-ISOBAR-DFF calculations

1. *Protons*: Examination of the data in Table V indicates that the VEGAS-DFF codes do a reasonably good job in predicting the features of the proton reactions. The calculations yield higher cross sections at large $\Delta A$ than those observed, and also tend to shift the centroids of the isotopic yields to smaller $A$ (i.e., higher yields of neutron-deficient products). The latter effect may be the chief cause of the former. These two deviations from observations may be due to the proton reactions occurring deeper in the nucleus in the calculated case than occurs in nature. The sums of the calculated cross sections are consistently higher than the measured results.

2. *Pions*: Examination of Fig. 1 demonstrates that the ISOBAR-DFF codes reproduce the energy dependence of the pion excitation functions. However, some rather large departures do exist and they are: (i) While experiment indicates that the sums of the $\pi^-$ cross sections are larger by about 10% than sums of the $\pi^+$ cross sections, the calculations indicate the converse to be true (Fig. 2). (ii) The calculated cross sections are in general too low at incident pion energies < 190 MeV and this difference increases as the pion energy is decreased. Proposed inclusion of $l=0$ partial waves in the calculations directed at the absorption process may increase the calculated cross sections at lower energy. (iii) The calculated isotopic yields of the Sc isotopes peak at $A=47$ while we observe the maximum closer to stability at $A\sim 45$. Products this far from the target ($\Delta A\sim 20$) are produced by evaporation of many particles following the intranuclear cascade and it appears that the DFF evaporation code may be overly influenced by the $N=28$ neutron shell. More sophisticated evaporation codes such as that of Hillman and Eyal[24] may more properly treat shell structure effects and yield better agreement.

### ACKNOWLEDGMENTS

We gratefully acknowledge the work of the LAMPF technical staff and operating crews for enabling the target irradiations to be carried out. Our gratitude is expressed to J. N. Ginocchio for his numerous VEGAS calculations and many helpful discussions relevant to our experimental results. Also, the useful discussions with J. Cumming concerning the interpretation of our results is acknowledged.

[1]C. K. Garrett and A. L. Turkevich, Phys. Rev. C 8, 594 (1973).
[2]H. R. Heydegger, C. K. Garrett, and A. Van Ginneken, Phys. Rev. C 6, 1235 (1972).
[3]P. L. Reeder, Ph.D. dissertation, University of California at Berkeley, Report No. UCRL-10531, 1962 (unpublished).
[4]R. L. Brodzinski, L. A. Rancitelli, J. A. Cooper, and

N. A. Wogman, Phys. Rev. C 4, 1250, 1257 (1971).
[5]J. E. Cline and E. B. Nieschmidt, Nucl. Phys. A 169, 437 (1971).
[6]G. V. S. Rayudu, J. Inorg. Nucl. Chem. 30, 2311 (1968).
[7]C. J. Orth, H. A. O'Brien, Jr., M. E. Schillaci, B. J. Dropesky, J. E. Cline, E. B. Nieschmidt, and R. L. Brodzinski, J. Inorg. Nucl. Chem. 38, 13 (1976).
[8]K. Chen, Z. Fraenkel, G. Friedlander, J. R. Grover, J. M. Miller, and Y. Shimamoto, Phys. Rev. 166, 949 (1968).
[9]K. Chen, G. Friedlander, and J. M. Miller, Phys. Rev. 176, 1208 (1968).
[10]K. Chen, G. Friedlander, G. D. Harp, and J. M. Miller, Phys. Rev. C 4, 2234 (1971).
[11]I. Dostrovsky, Z. Fraenkel, and G. Friedlander, Phys. Rev. 116, 683 (1959).
[12]T. T. Sugihara and W. F. Libby, Phys. Rev. 88, 587 (1952).
[13]A. L. Turkevich and S. Fong, Phys. Rev. 92, 521 (1953).
[14]A. L. Turkevich and J. B. Niday, Phys. Rev. 90, 342 (1953).
[15]L. Winsberg, Phys. Rev. 95, 198 (1954).
[16]N. Sugarman and A. Haber, Phys. Rev. 92, 730 (1953).
[17]G. D. Harp, K. Chen, G. Friedlander, Z. Fraenkel, and and J. M. Miller, Phys. Rev. C 8, 581 (1973).
[18]B. J. Dropesky, G. W. Butler, C. J. Orth, R. A. Williams, G. Friedlander, M. A. Yates, and S. B. Kaufman, Phys. Rev. Lett. 34, 821 (1975).
[19]R. A. Williams, C. J. Orth, G. W. Butler, G. C. Giesler, M. A. Yates-Williams, and B. J. Dropesky (unpublished).
[20]G. Kuhl and U. Kneissl, Nucl. Phys. A 195, 559 (1972).
[21]C. J. Orth, W. R. Daniels, B. J. Dropesky, R. A. Williams, G. C. Giesler, and J. N. Ginocchio (unpublished).
[22]J. B. Cumming, Annu. Rev. Nucl. Sci. 13, 261 (1963).
[23]The center of development of the VEGAS-ISOBAR intranuclear cascade code was transferred from the Brookhaven National Laboratory, where it was originated, to the Los Alamos Scientific Laboratory by G. D. Harp in 1974. J. N. Ginocchio is now in charge of the program to improve, test, and apply this code, which is followed by the DFF evaporation code. See J. N. Ginocchio, Phys. Rev. C 17, 195 (1978).
[24]M. Hillman and Y. Eyal, in Proceedings of the American Chemical Society 174th National Meeting, Chicago, Aug. 29–Sept. 2, 1977 (unpublished); Abstract No. 47, Nuclear Chemistry and Technology Bulletin.